

Order parameter symmetries for magnetic and superconducting instabilities: Bethe-Salpeter analysis of functional renormalization-group solutions

A. A. Katanin, Arno P. Kampf

Angaben zur Veröffentlichung / Publication details:

Katanin, A. A., and Arno P. Kampf. 2005. "Order parameter symmetries for magnetic and superconducting instabilities: Bethe-Salpeter analysis of functional renormalization-group solutions." *Physical Review B* 72 (20): 250128.
<https://doi.org/10.1103/PhysRevB.72.205128>.

Order-parameter symmetries for magnetic and superconducting instabilities: Bethe-Salpeter analysis of functional renormalization-group solutions

A. A. Katanin

Max-Planck-Institut für Festkörperforschung, D-70569 Stuttgart, Germany
and Institute of Metal Physics, 620219 Ekaterinburg, Russia

A. P. Kampf

Theoretische Physik III, Elektronische Korrelationen und Magnetismus, Institut für Physik, Universität Augsburg,
D-86135 Augsburg, Germany

(Received 14 June 2005; revised manuscript received 13 September 2005; published 30 November 2005)

The Bethe-Salpeter equation is combined with the temperature-cutoff functional renormalization group approach to analyze the order parameter structure for the leading instabilities of the 2D t - t' Hubbard model. We find significant deviations from the conventional s -, p -, or d -wave forms, which is due to the frustration of antiferromagnetism at small and intermediate t' . With adding a direct antiferromagnetic spin-exchange coupling the eigenfunctions in the particle-hole channel have extended s -wave form, while in the particle-particle singlet pairing channel a higher angular momentum component arises besides the standard $d_{x^2-y^2}$ wave component, which flattens the angular dependence of the gap. For t' closer to $t/2$ we find a delicate competition of ferromagnetism and triplet pairing with a nontrivial pair-wavefunction.

DOI: 10.1103/PhysRevB.72.205128

PACS number(s): 71.27.+a, 71.10.Fd, 74.20.Rp, 74.25.Dw

It is by now well established that the superconducting order parameter in high- T_c compounds is well described by a $(\cos k_x - \cos k_y)$ -momentum dependence; it is largest at the Fermi surface (FS) points close to $(\pi, 0)$ and $(0, \pi)$ and vanishes at the FS crossings on the Brillouin zone (BZ) diagonals. Accurate measurements of the gap function, however, revealed a slight deviation from this $d_{x^2-y^2}$ -wave momentum dependence,¹ with a flatter angular dependence near the nodal points. The symmetry and the details of the momentum dependence of the superconducting order parameter are closely related to the structure of the effective attractive interaction between the electrons. The precise momentum dependence of the energy gap therefore contains valuable information about the underlying pairing mechanism, for which antiferromagnetic (AFM) spin fluctuations are a viable candidate for cuprates.²⁻⁵

Another type of unconventional superconductor is the layered ruthenate Sr_2RuO_4 ,⁶ which most likely has triplet pairing with p -wave symmetry.⁷ It was proposed that the pairing in this material results from ferromagnetic (FM) spin fluctuations.^{8,9} Although inelastic neutron scattering has so far been unsuccessful to detect significant low-energy FM spin fluctuations,¹⁰ this idea finds support from the enhanced tendencies towards ferromagnetism in the electron doped compound $\text{Sr}_{2-x}\text{La}_x\text{RuO}_4$ (Ref. 11) and in isoelectronic Ca_2RuO_4 under hydrostatic pressure.¹²

The important role of AFM and FM fluctuations as a possible driving source of singlet and triplet superconductivity, respectively, was emphasized early on in the pioneering work in Refs. 13–15. Recently, the interplay of antiferromagnetism and d -wave superconductivity (d SC) and ferromagnetism and p -wave superconductivity (p SC), respectively, was reconsidered within the t - t' Hubbard model using functional renormalization-group (fRG) techniques.¹⁶⁻²⁰ Early versions of fRG,¹⁶⁻¹⁸ which used the momentum cutoff pro-

cedure, were unable to search for ferromagnetism. This drawback is overcome in the temperature-cutoff fRG approach (TCRG),¹⁹ which proved successful in describing both, AFM and FM instabilities together with singlet- and triplet superconducting pairing in the weak-coupling t - t' Hubbard model and its extensions in a broad parameter range.¹⁹⁻²¹ In the previous fRG analyses it has been a common practice to assume order parameter structures, which have the form of square lattice basis functions with s -, p - or d -wave symmetry.¹⁶⁻²¹ Although it was recognized that in the RG flow of the order parameter susceptibilities also the momentum dependence acquires specific corrections to their initial form,^{17,19-22} these corrections were so far not analyzed in detail. Indeed, actual order parameter structures may have admixtures of different symmetry components, and it is necessary to develop an unbiased method to determine their precise momentum dependence.

In the present paper we use the Bethe-Salpeter equations to extract eigenfunctions and eigenvalues of the effective interaction in the particle-particle (pp) or the particle-hole (ph) channel—similarly as in previous quantum Monte Carlo studies.²³ Here we consider a combination of the Bethe-Salpeter equations and the fRG approach. We choose the TCRG version¹⁹ as the most suitable tool, because the effective model obtained within this scheme does not contain any unintegrated degrees of freedom even at the intermediate stages of the RG flow.

We apply this procedure to identify the order parameter structure for the leading instabilities of the 2D t - t' extended Hubbard model $H_\mu = H - (\mu - 4t')N$ with

$$H = - \sum_{ij\sigma} t_{ij} c_{i\sigma}^\dagger c_{j\sigma} + U \sum_i n_{i\uparrow} n_{i\downarrow} + J \sum_{\langle ij \rangle} \mathbf{S}_i \cdot \mathbf{S}_j, \quad (1)$$

where $t_{ij} = t$ for nearest neighbor (nn) sites i and j and $t_{ij} = -t'$ for next-nn sites ($t, t' > 0$) on a square lattice; for conve-

nience we have shifted the chemical potential μ by $4t'$. In Eq. (1) we have included a direct nn spin exchange interaction J ; $S_i = c_{i\alpha}^\dagger \boldsymbol{\sigma}_{\alpha\beta} c_{i\beta}/2$, and $\boldsymbol{\sigma}$ denotes the Pauli matrices. While such an interaction is generated from the on-site Coulomb repulsion at strong-coupling, we add it here as an independent interaction in the weak-coupling regime, where the RG scheme is applicable.

We follow the many-patch fRG version for one-particle irreducible Green functions as proposed in Ref. 19. This TCRG scheme uses the temperature as a natural cutoff parameter and accounts for excitations with momenta far from and close to the FS, which is necessary for the description of instabilities arising from zero-momentum ph scattering, e.g., ferromagnetism. Neglecting the frequency dependence of the vertices, which is expected to have minor relevance in the weak-coupling regime, the RG differential equation for the interaction vertex has the form¹⁹

$$\frac{dV_T}{dT} = -V_T \circ \frac{dL_{pp}}{dT} \circ V_T + V_T \circ \frac{dL_{ph}}{dT} \circ V_T, \quad (2)$$

where \circ is a short notation for summations over intermediate momenta and spin,

$$L_{ph,pp}(\mathbf{k}, \mathbf{k}') = \frac{f_T(\varepsilon_{\mathbf{k}}) - f_T(\pm\varepsilon_{\mathbf{k}'})}{\varepsilon_{\mathbf{k}} \mp \varepsilon_{\mathbf{k}'}} \quad (3)$$

and $f_T(\varepsilon)$ is the Fermi function. The upper sign in Eq. (3) is for L_{ph} and the lower sign for L_{pp} , respectively. Equation (2) has to be solved with the initial condition $V_{T_0}(\mathbf{k}_1, \mathbf{k}_2, \mathbf{k}_3, \mathbf{k}_4) = U$; the initial temperature is chosen as large as $T_0 = 400t$.

We discretize the momentum space in $N_p = 48$ patches using the same patching scheme as in Ref. 19. This reduces the integro-differential equations (2) and (4) to a set of 5824 differential equations, which were solved numerically. The evolution of the vertices with decreasing temperature determines the temperature dependence of the susceptibilities according to^{19,24}

$$\begin{aligned} \frac{d\chi_{m,r}}{dT} &= \sum_{\mathbf{k}'} \mathcal{R}_{\mathbf{k}'}^{m,r} \mathcal{R}_{\mp\mathbf{k}'+\mathbf{q}_m}^{m,r} \frac{dL_{pp,ph}(\mathbf{k}', \mp\mathbf{k}'+\mathbf{q}_m)}{dT}, \\ \frac{d\mathcal{R}_{\mathbf{k}}^{m,r}}{dT} &= \mp \sum_{\mathbf{k}'} \mathcal{R}_{\mathbf{k}'}^{m,r} \Gamma_m^T(\mathbf{k}, \mathbf{k}') \frac{dL_{pp,ph}(\mathbf{k}', \mp\mathbf{k}'+\mathbf{q}_m)}{dT}, \end{aligned} \quad (4)$$

where

$$\begin{aligned} \Gamma_m^T(\mathbf{k}, \mathbf{k}') &= \begin{cases} V_T(\mathbf{k}, \mathbf{k}', \mathbf{k}'+\mathbf{q}_m) - 2V_T(\mathbf{k}, \mathbf{k}', \mathbf{k}+\mathbf{q}_m) & \text{phc (PI, DDW),} \\ V_T(\mathbf{k}, \mathbf{k}', \mathbf{k}'+\mathbf{q}_m) & \text{phs (AFM, FM),} \\ V_T(\mathbf{k}, -\mathbf{k}+\mathbf{q}_m, \mathbf{k}') & \text{pp (dSC, pSC).} \end{cases} \\ & \quad (5) \end{aligned}$$

m denotes one of the possible channels: ph spin (phs), which traces FM and AFM instabilities, ph charge (phc) for the Pomeranchuk instability (PI) (Ref. 25 or d -density wave (DDW)),²⁶ or pp for superconducting singlet and triplet insta-

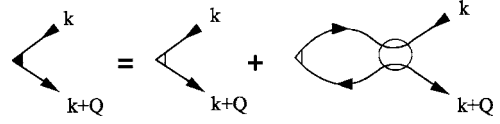


FIG. 1. Diagrammatic representation of the three-point vertex $\mathcal{R}_{\mathbf{k}}^{m,r}$ (solid triangle), which has the structure of a vertex diagram in a static external field acting in the channel m with the r th initial vertex function $f_{\mathbf{k}}^{(r)}$ defined in Eq. (6) and shown as an open triangle. The specific example shows the phsQ channel. The circle represents the reducible electron-electron interaction vertex.

bilities; $\mathbf{q}_m = \mathbf{Q} = (\pi, \pi)$ for AFM and DDW and $\mathbf{q}_m = \mathbf{0}$ otherwise. In the following we use the notation $m\mathbf{q}_m$ to denote the specific channel. The index r in Eq. (4) represents the symmetry of the corresponding channel. The upper signs and pp-indices in Eq. (4) refer to the superconducting instabilities (d SC and p SC), and the lower signs and ph-indices refer to the charge and magnetic instabilities.

The three-point vertices $\mathcal{R}_{\mathbf{k}}^{m,r}$ can be considered as vertices describing the propagation of the electron in a static external field; their diagrammatic representation is shown in Fig. 1. The initial conditions at T_0 for Eqs. (4) are $\mathcal{R}_{\mathbf{k}}^{m,r} = f_{\mathbf{k}}^{(r)}$ and $\chi_{m,r} = 0$, where the function $f_{\mathbf{k}}^{(r)}$ belongs to one of the irreducible representations of the point group of the square lattice (A_{1g} or $B_{1,2g}$), e.g.,

$$f_{\mathbf{k}}^{(r)} = A^{-1} \begin{cases} \cos k_x - \cos k_y & d_{x^2-y^2}\text{-wave} & (B_{1g}), \\ \sin k_{x(y)} & p\text{-wave} & (B_{2g}), \\ 1 & s\text{-wave} & (A_{1g}), \end{cases} \quad (6)$$

with a normalization coefficient $A = (1/N) \sum_{\mathbf{k}} f_{\mathbf{k}}^2$. The momentum dependence of the vertices $\mathcal{R}_{\mathbf{k}}^{m,r}$ changes during the RG flow and at low temperatures it is expected to reflect the momentum dependence of the ground-state order parameter of the selected symmetry. However, these vertex functions depend on the initial choice of the functions $f_{\mathbf{k}}^{(r)}$, and therefore they cannot serve as an unbiased tool to obtain the structure of the ground-state order parameters.

To perform an alternative analysis, which is not based on the knowledge of the wave functions at high temperatures, we consider the solution of the Bethe-Salpeter equations²³

$$\begin{aligned} \sum_{\mathbf{p}} \bar{\Gamma}_{ph}(\mathbf{k}, \mathbf{p}; \mathbf{p}, \mathbf{k}) L_{ph}(\mathbf{p}, \mathbf{p} + \mathbf{q}_m) \phi_{\mathbf{p}}^{ph} &= \lambda_{ph} \phi_{\mathbf{k}}^{ph}, \\ - \sum_{\mathbf{p}} \bar{\Gamma}_{pp}(\mathbf{k}, \mathbf{p}; \mathbf{p}, \mathbf{k}) L_{pp}(\mathbf{p}, \mathbf{p}) \phi_{\mathbf{p}}^{pp} &= \lambda_{pp} \phi_{\mathbf{k}}^{pp}, \end{aligned} \quad (7)$$

where $\bar{\Gamma}_{ph}$ and $\bar{\Gamma}_{pp}$ denote irreducible vertices in ph and pp channels, respectively. Exploiting the connection to reducible vertices, Eqs. (7) can be rewritten as²³

$$\sum_{\mathbf{p}} \Gamma_m^T(\mathbf{k}, \mathbf{p}) L_{ph,pp}^T(\mathbf{p}, \pm\mathbf{p} + \mathbf{q}_m) \phi_{\mathbf{p}}^{m,l} = \frac{\lambda_{m,l} \phi_{\mathbf{k}}^{m,l}}{1 - \lambda_{m,l}}, \quad (8)$$

where l enumerates eigenvalues and $-$ functions for a given channel m . The reducible vertices $\Gamma_m^T(\mathbf{k}, \mathbf{p})$ can be directly extracted from the fRG flow according to Eq. (5).

The value $\lambda_{m,l} = 1$ corresponds to an ordering instability

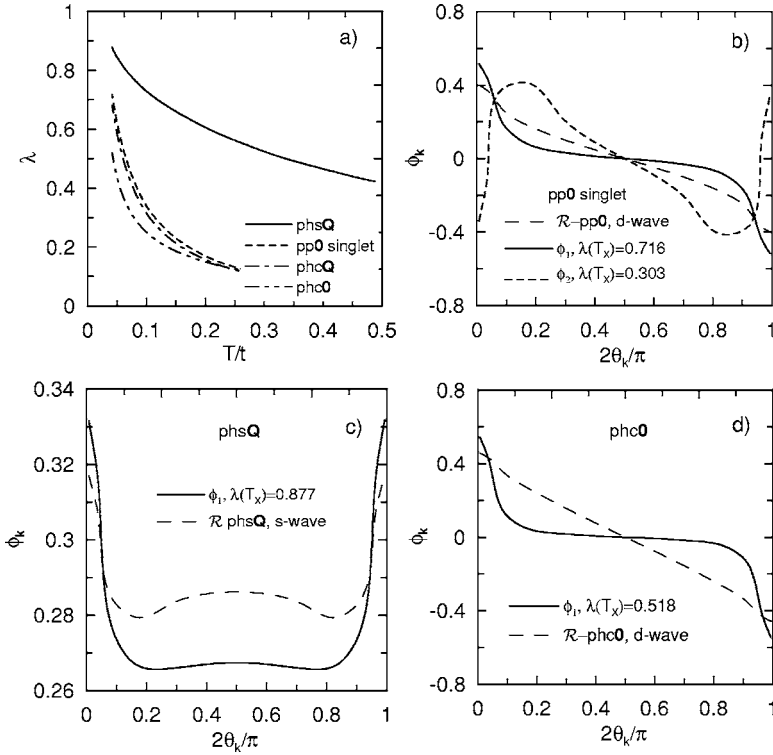


FIG. 2. Eigenvalues (a) and angular θ_{k_f} -dependence on the FS of the eigenfunctions $\phi_{\mathbf{k}}^{m,l} = \phi_l$ of the Bethe-Salpeter equation and the normalized three-point vertices $\mathcal{R}_{\mathbf{k}}^{m,r}$ (denoted as $\mathcal{R}-m,r$) at $T=T_X$ (b,c,d) for $t'=0.1t$, $U=2t$, $J=\mu=0$. T_X is the lowest temperature reached in the fRG flow [see (a)].

with the symmetry of the eigenfunction $\phi_{\mathbf{k}}^{m,l}$. Therefore, tracing the temperature dependence of eigenvalues and -functions allows to identify both, the leading instabilities *and* their concomitant order parameter structure. We stop the fRG flow at the temperature T_X , where the maximum interaction vertex $V_{\max} \equiv \max\{V(\mathbf{k}_1, \mathbf{k}_2; \mathbf{k}_3, \mathbf{k}_4)\}$ reaches the value $20t$. T_X should be understood as a crossover temperature into a renormalized classical regime with exponentially large correlation length,²¹ we have verified that the following results for the eigenfunctions are only weakly dependent on the choice of T_X .

Eigenfunctions and eigenvalues of the Bethe-Salpeter equations provide more detailed information than can be obtained from the momentum dependence of the three-point vertices $\mathcal{R}_{\mathbf{k}}^{m,r}$, which determine the order-parameter susceptibilities according to Eq. (4). Unlike the vertices $\mathcal{R}_{\mathbf{k}}^{m,r}$, the solutions of the Bethe-Salpeter equations do not depend on the initial choice of the functions $f_{\mathbf{k}}^{(r)}$ and, therefore, do not require *a priori* the knowledge of the symmetry of the leading instability.

The three-point vertices

$$\tilde{\mathcal{R}}_{\mathbf{k}}^{m,r} = f_{\mathbf{k}}^{(r)} + \sum_{\mathbf{p}} \Gamma_m^T(\mathbf{k}, \mathbf{p}) L_{\text{ph,pp}}^T(\mathbf{p}, \pm \mathbf{p} + \mathbf{q}_m) f_{\mathbf{p}}^{(r)} \quad (9)$$

described by the diagram of Fig. 1 can be obtained directly from the solutions of the Bethe-Salpeter equations. Expanding the functions $f_{\mathbf{k}}^{(r)}$ in terms of eigenfunctions of the Bethe-Salpeter equation and using Eq. (8), we obtain

$$\tilde{\mathcal{R}}_{\mathbf{k}}^{m,r} = \sum_l \frac{\phi_{\mathbf{k}}^{m,l}}{1 - \lambda_{m,l}} \sum_{\mathbf{k}'} f_{\mathbf{k}'}^{(r)} \phi_{\mathbf{k}'}^{m,l}. \quad (10)$$

The vertices $\tilde{\mathcal{R}}_{\mathbf{k}}^{m,r}$ found in this way, however, do not necessarily coincide with those obtained directly from the RG pro-

cedure, Eq. (4), because generally the one-loop approximation does not exactly reproduce the solution of the corresponding Bethe-Salpeter equation. The only case when the three-point vertices $\mathcal{R}_{\mathbf{k}}^{m,r}$ and $\tilde{\mathcal{R}}_{\mathbf{k}}^{m,r}$ coincide is the ladder approximation when either only the pp-channel or one of the ph-channels in Eq. (2) is retained. Nevertheless, as we will see below, the results for the vertex $\mathcal{R}_{\mathbf{k}}^{m,r}$ from Eqs. (4) are qualitatively similar to those found from Eq. (10).

It is clearly established from Eq. (10) that $\tilde{\mathcal{R}}_{\mathbf{k}}^{m,r}$ (and similarly $\mathcal{R}_{\mathbf{k}}^{m,r}$) is actually a mixture of different eigenfunctions $\phi_{\mathbf{k}}^{m,l}$, whose weights are proportional to $1/(1 - \lambda_{m,l})$ with coefficients determined by the overlap of the eigenfunction with $f_{\mathbf{k}'}^{(r)}$. If one of the eigenvalues $\lambda_{m,l}$ is much closer to unity than all the others, the corresponding term in the sum over l in Eq. (10) is expected to dominate and $\tilde{\mathcal{R}}_{\mathbf{k}}^{m,r}$ essentially coincides with the corresponding eigenfunction $\phi_{\mathbf{k}}^{m,l}$.

Below we discuss the results of the numerical solution of the Bethe-Salpeter equations and compare them to the results for the three-point vertices $\mathcal{R}_{\mathbf{k}}^{m,r}$ for different parameter regimes. We start in Fig. 2 with results at the van Hove (vH) band filling ($\mu=0$) for small $t'=0.1t$, $J=0$, and $U=2t$. The AFM pqsQ instability has the largest eigenvalue at T_X in agreement with previous fRG work based on the analysis of order parameter susceptibilities.¹⁹ The corresponding eigenfunction [Fig. 2(c)] has a slight variation around the FS with an enhancement near $(\pi, 0)$ and $(0, \pi)$, which most likely originates from the vH singularity nature of these points. The eigenfunctions in the subleading phc0 and pp0 channels are sizable near $(\pi, 0)$ and $(0, \pi)$ only. Although the eigenvalue of the zero-momentum ph instability in the charge channel (phc0) is relatively small at $T=T_X$ ($\lambda \approx 0.5$), it rapidly increases at low temperatures. The corresponding eigenfunction [Fig. 2(d)] is antisymmetric with respect to 90° rotation,

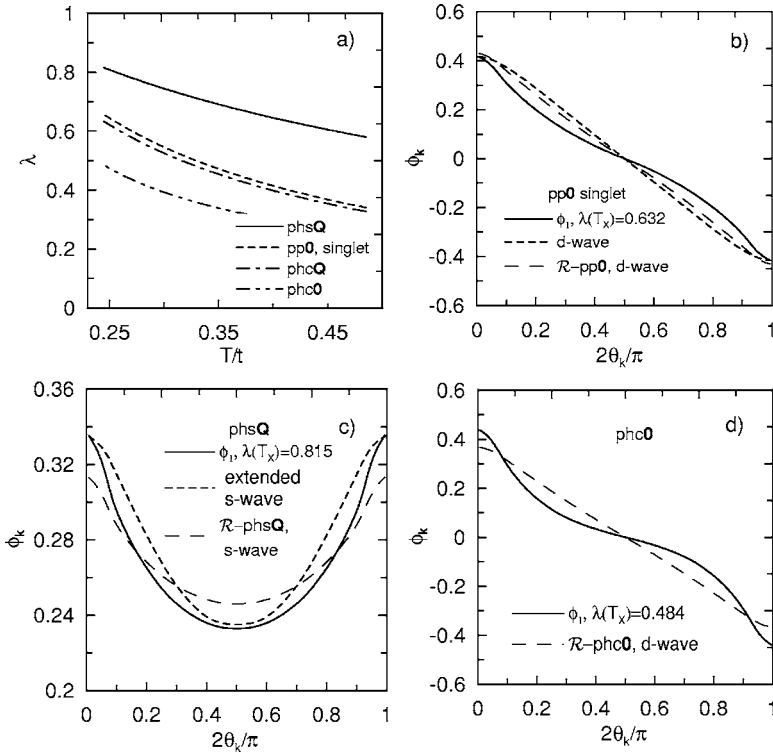


FIG. 3. Same as in Fig. 2 for $U=1.5t$, $J=0.3t$.

thus providing the possibility for the Pomeranchuk instability with a spontaneous d -wavelike deformation of the FS.^{27,28} The eigenvalues for the PI at $t'=0.1t$ are larger than those at $t'=0$ (not shown), which supports the conclusion of Ref. 28, that a finite value of t' at vH band fillings enhances the tendency towards a Pomeranchuk instability.

The momentum dependence of the three-point vertices $\mathcal{R}_k^{m,r}$ is qualitatively similar to the leading eigenfunctions in the pp0 and pqsQ channels, however with a smaller variation around the FS. In the phc0 channel we observe a stronger difference of the vertex $\mathcal{R}_k^{\text{phc},d\text{-wave}}$, which has almost the $d_{x^2-y^2}$ -wave form, from the corresponding eigenfunction of the Bethe-Salpeter equation.

To investigate the role of t' -induced frustration of antiferromagnetism, we turn on a small direct exchange interaction $J=0.3t$ to strengthen the AFM correlations, and decrease simultaneously the value of U to $1.5t$ in order to remain in the weak-coupling regime. Figure 3 shows the resulting changes. At finite J the eigenfunctions in the pp0 and phc0 channels are essentially nonzero all around the FS, however they are flatter than the $d_{x^2-y^2}$ -wave function. The eigenfunction in the pqsQ channel is of extended s -wave form. The eigenvalue for the phc0 channel is smaller than at $J=0$, implying that stronger antiferromagnetism weakens the tendency towards a Pomeranchuk instability. Similarly to the $J=0$ case, we observe a smaller variation of the vertices $\mathcal{R}_k^{m,r}$ around the FS, than in the momentum dependence of the corresponding eigenfunctions of the Bethe-Salpeter equation.

With increasing t' to $0.3t$ (Fig. 4) the largest eigenvalue occurs in the singlet dSC (pp0 singlet) channel. The corresponding pair wave function maintains its shape with a slight deviation from the $(\cos k_x - \cos k_y)$ -form, i.e., a flattening near the BZ diagonal. In the pqsQ and phc0 channels we observe again a weaker momentum variation of $\mathcal{R}_k^{m,r}$. The

vertex $\mathcal{R}_k^{\text{pp0},d\text{-wave}}$ instead is very close to the shape of the corresponding Bethe-Salpeter eigenfunctions in the pp0 channel.

For $t'=0.45t$ a ferromagnetic instability is expected,^{19,20} and we start again with the vH band filling case for $\mu=0$ (Fig. 5). We increase the interaction strength to $U=3t$, since the corresponding crossover temperatures for the FM instability are lower. The largest Bethe-Salpeter eigenvalues [Fig. 5(a)] arise in the FM (pqs0), p SC (pp0 triplet) and AFM channels (pqsQ). Remarkably, the wave function in the *triplet* pp0 channel deviates significantly from the $\sin k_x$ form [see Fig. 5(b)], but its eigenvalue remains smaller than the eigenvalue for ferromagnetism. This deviation is also well reproduced by the corresponding momentum dependence of the vertex $\mathcal{R}_k^{\text{pp0},p\text{-wave}}$.

On moving away from the vH band filling at $t'=0.45t$, we observe a further increase of the eigenvalue in the triplet pairing channel (Fig. 6), which however remains smaller than the eigenvalue of the ferromagnetic instability at the lowest temperature we can safely reach in the fRG flow. Simultaneously, the eigenfunction in the triplet superconducting (pp0) channel slightly distorts towards the wave function $f_k^{(p\text{-wave})}$, but strong deviations persist in both, the eigenfunction of the Bethe-Salpeter equation and the vertex $\mathcal{R}_k^{\text{pp0},p\text{-wave}}$. Singlet superconductivity (pp0 singlet channel), which was not among the dominant instabilities at $\mu=0$, is also significantly enhanced for $\mu>0$. There are two eigenfunctions, which are symmetric and antisymmetric with respect to reflection at the BZ diagonal with almost equal eigenvalues in the pp singlet channel. Both eigenfunctions are essentially nonzero at $(\pi, 0)$ and $(0, \pi)$ only, and therefore not expected to be stabilized thermodynamically. Because of the presence of two nearly-degenerate eigenfunctions, the three-point vertex $\mathcal{R}_k^{\text{pp0},d\text{-wave}}$ in this case substantially devi-

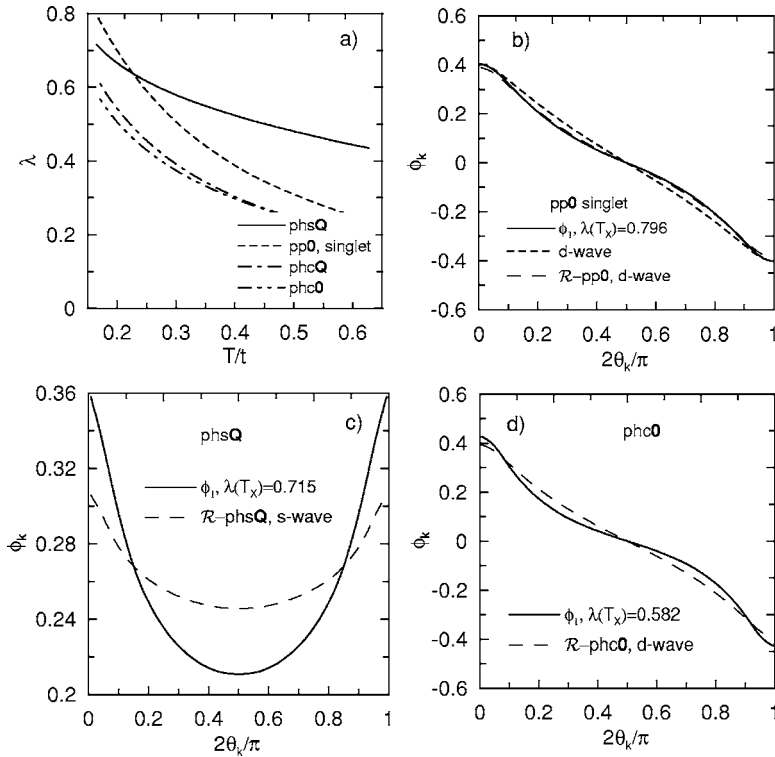


FIG. 4. Same as in Fig. 2 for $t'=0.3t$, $U=2t$, $J=0.3t$.

ates from the momentum dependence of the leading eigenfunction.

In conclusion, we have investigated the symmetry of the leading instabilities of the 2D t - t' Hubbard model using as a novel tool the combination of the Bethe-Salpeter equation and the fRG approach. Although in most cases the leading instabilities coincide with those from susceptibility based

analyses, the true shape of the eigenfunctions significantly differs from the s -, p - or d -wave basis functions. At small t' we find in particular a flattening of the eigenfunction in the pairing $pp0$ channel near the nodes—in qualitative agreement with experimental data for cuprates.¹ The addition of a direct spin exchange interaction to the Hubbard model at weak-coupling was essential to reproduce a

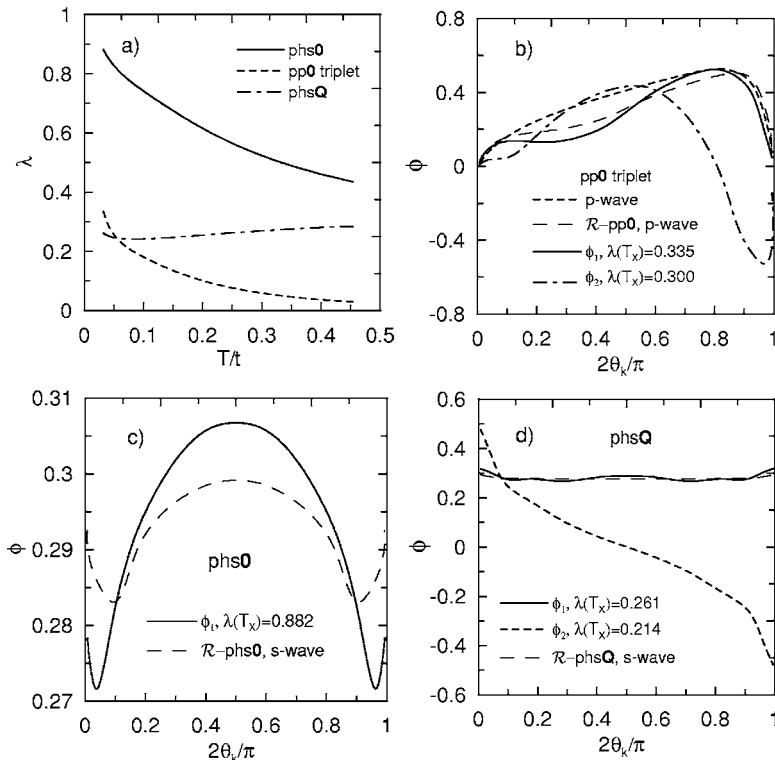


FIG. 5. Same as in Fig. 2 for $t'=0.45t$, $U=3t$.

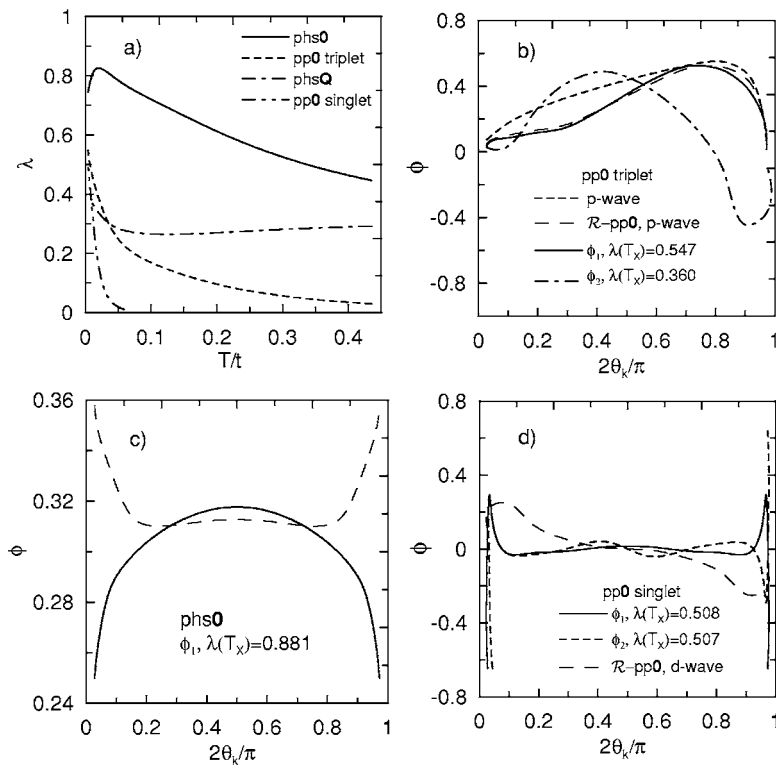


FIG. 6. Same as in Fig. 2 for $t'=0.45t$, $U=3t$, and $\mu=0.035t$.

($\cos k_x - \cos k_y$)-like form of the superconducting gap at low and intermediate t' . The instability towards triplet pairing at larger t' also shows a substantial deviation from the standard p -wave $\sin k_x$ -form. In many cases we have investigated, the eigenfunctions of the Bethe-Salpeter equations strongly deviate from the corresponding three-point vertices $\mathcal{R}_k^{m,r}$, which enter the order parameter susceptibilities, due to either a qualitative difference of the eigenfunctions from the basis functions $f_k^{(s,p,d)\text{-wave}}$ or the presence of several almost degen-

erate eigenfunctions. The proposed new technique may prove most useful in future studies of magnetic and superconducting instabilities without presupposing a special momentum dependence of the candidate order parameters.

This work was supported by the Deutsche Forschungsgemeinschaft through SFB 484. We gratefully acknowledge discussions with D. J. Scalapino, W. Metzner, C. Honerkamp, and A. Castro-Neto.

- ¹J. Mesot, M. R. Norman, H. Ding, M. Randeria, J. C. Campuzano, A. Paramekanti, H. M. Fretwell, A. Kaminski, T. Takeuchi, T. Yokoya, T. Sato, T. Takahashi, T. Mochiku, and K. Kadowaki, Phys. Rev. Lett. **83**, 840 (1999).
- ²D. J. Scalapino, J. Low Temp. Phys. **117**, 179 (1999).
- ³N. E. Bickers, D. J. Scalapino, and S. R. White, Phys. Rev. Lett. **62**, 961 (1989).
- ⁴J. Schmalian, D. Pines, and B. Stojkovic, Phys. Rev. Lett. **80**, 3839 (1998).
- ⁵A. Chubukov and D. Morr, Phys. Rep. **288**, 355 (1997); A. Abanov and A. V. Chubukov, Phys. Rev. Lett. **84**, 5608 (2000).
- ⁶Y. Maeno, T. M. Rice, and M. Sgrist, Phys. Today **54** (1), 42 (2001).
- ⁷K. Deguchi, Z. Q. Mao, and Y. Maeno, J. Phys. Soc. Jpn. **73**, 1313 (2004).
- ⁸I. I. Mazin and D. Singh, Phys. Rev. Lett. **79**, 733 (1997); **82**, 4324 (1999).
- ⁹S. Murakami, N. Nagaosa, and M. Sgrist, Phys. Rev. Lett. **82**, 2939 (1999).
- ¹⁰Y. Sidis, M. Braden, P. Bourges, B. Hennion, S. NishiZaki, Y. Maeno, and Y. Mori, Phys. Rev. Lett. **83**, 3320 (1999).
- ¹¹N. Kikugawa and Y. Maeno, cond-mat/0211248 (unpublished).
- ¹²F. Nakamura, T. Goko, M. Ito, T. Fujita, S. Nakatsuji, H. Fukazawa, Y. Maeno, P. Alireza, D. Forsythe, and S. R. Julian, Phys. Rev. B **65**, 220402(R) (2002).
- ¹³W. Kohn and J. M. Luttinger, Phys. Rev. Lett. **15**, 524 (1965).
- ¹⁴N. F. Berk and J. R. Schrieffer, Phys. Rev. Lett. **17**, 433 (1966).
- ¹⁵D. J. Scalapino, E. Loh, Jr., and J. E. Hirsch, Phys. Rev. B **34**, 8190 (1986); **35**, 6694 (1987).
- ¹⁶D. Zanchi and H. J. Schulz, Phys. Rev. B **54**, 9509 (1996); **61**, 13609 (2000).
- ¹⁷C. J. Halboth and W. Metzner, Phys. Rev. B **61**, 7364 (2000).
- ¹⁸C. Honerkamp, M. Salmhofer, N. Furukawa, and T. M. Rice, Phys. Rev. B **63**, 035109 (2001).
- ¹⁹C. Honerkamp and M. Salmhofer, Phys. Rev. Lett. **87**, 187004 (2001); Phys. Rev. B **64**, 184516 (2001).
- ²⁰A. A. Katanin and A. P. Kampf, Phys. Rev. B **68**, 195101 (2003).
- ²¹A. P. Kampf and A. A. Katanin, Phys. Rev. B **67**, 125104 (2003).

- ²²See also the renormalized perturbation theory analysis of A. Neumayr and W. Metzner, Phys. Rev. B **67**, 035112 (2003).
- ²³N. Bulut, D. J. Scalapino, and S. R. White, Phys. Rev. B **47**, 6157 (1993); **47**, 14599 (1993).
- ²⁴C. Honerkamp, M. Salmhofer, and T. M. Rice, Eur. Phys. J. B **27**, 127 (2002).
- ²⁵I. J. Pomeranchuk, Sov. Phys. JETP **8**, 361 (1958).
- ²⁶S. Chakravarty, R. B. Laughlin, D. K. Morr, and C. Nayak, Phys. Rev. B **63**, 094503 (2001).
- ²⁷H. Yamase and H. Kohno, J. Phys. Soc. Jpn. **69**, 332 (2000); **69**, 2151 (2000).
- ²⁸C. J. Halboth and W. Metzner, Phys. Rev. Lett. **85**, 5162 (2000).